Received: 28 January 2023 | Revised: 18 June 2023 | Accepted: 21 June 2023

DOI: 10.1002/mp.16610

RESEARCH ARTICLE

MEDICAL PHYSICS

Construction and dosimetric characterization of a motorized scanning-slit system for electron FLASH experiments

Roxane Oesterle | **Claude Bailat** | **Damien Buhlmann** | **Francois Bochud** | **Veljko Grilj**

Institute of Radiation Physics, Lausanne University Hospital, Lausanne, Switzerland

Correspondence
Veljko Grilj, Institute of Radiation Physics, Lausanne University Hospital, Rue du Grand-Pre 1, 1007 Lausanne, Switzerland.
Email: veljko.grilj@chuv.ch

Funding information
FNS CRS, Grant/Award Number: II5_186369; NIH, Grant/Award Number: PO1CA244091; EMPIR, Grant/Award Number: 18HLT04 UHDpulse

Abstract

Background: Beam scanning is a useful technique for the treatment of large tumors when the primary beam size is limited, which is the case with radiation beams used in FLASH radiotherapy.

Purpose: To optimize beam scanning as a dose delivery method for FLASH radiotherapy, it is necessary to first understand the effects of beam scanning on the FLASH effect. To do so, biological FLASH experiments need to be done using defined beam parameters with beam scanning and compared to the situation without beam scanning. In this regard, we propose implementation of a simple slit scanning system with an electron FLASH beam to obtain a scanned radiation field that closely resembles a static field.

Methods: A pulsed electron linear accelerator (linac) was used in combination with a scanning slit system in order to simulate a scanned electron beam. Three configurations that produced homogeneous lateral profiles and high enough doses per pulse for FLASH experiments were established. The optimal scanning parameters were found for each configuration by examining the flatness of the obtained lateral dose profiles. Using the optimal scanning parameters, the scanned FLASH beams were dosimetrically characterized and compared to non-scanned open field beam.

Results: A final electron FLASH beam scanning configuration was found for a 1 mm wide slit at a distance of 350 mm from the linac and a 2 mm wide slit at distances of 350 and 490 mm from the linac. The lateral profiles for these final configurations were found to have a homogeneity that is comparable to the open field profiles. The percentage depth dose (PDD) values found for these final configurations closely matched (by a few percentage) the PDD of the open field beam.

Conclusions: Three electron FLASH beam scanning configurations achieved by the motorized slit system were found to produce radiation fields similar to a non-scanned open field electron beam. These final configurations can therefore be used in future biological FLASH experiments to compare to non-scanned beam experiments in order to optimize beam scanning as a technique permitting the treatment of larger tumors with FLASH radiotherapy.

KEYWORDS
beam scanning, FLASH, radiotherapy, slit collimator

1 | INTRODUCTION

Radiotherapy is a common treatment against all types of cancer; however, normal tissue toxicity is still a limiting factor in current radiotherapy treatments. A new emerging irradiation technique, called FLASH radiotherapy (FLASH-RT), has shown the potential to overcome these limitations. FLASH-RT is based on the FLASH effect, a biological effect discovered in 2014 where for certain ultra-high dose rate (UHDR, >100 Gy/s) configurations, there is an increase in differential response between tumor and normal tissues, meaning normal tissues are preserved while maintaining an equivalent or better efficacy against tumors as conventional (CONV, <10 Gy/min) radiotherapy.[1–6] The FLASH effect has since been proven in various tissues (e.g., lung,[4] brain,[7–10] gut,[11–13] skin[14]) and on various animal models (e.g., zebrafish,[15] mice,[8–13] cat,[16] pig[16]), leading to the treatment of the first human patient.[17] While most of the current research shows a promising potential of FLASH-RT, the exact mechanisms are not yet fully understood and most of the data have been done using small (<3 cm) field sizes. The field size is limited by the technology of delivering such a high dose-rate with currently available machines. One way to achieve bigger field sizes would be to scan a narrow beam over a large, desired surface. Scanning a narrow beam is already a technique used in clinical proton therapy, where the beam is scanned spot-by-spot.[18] By doing so, the dose absorbed at one point in the field comes from the field contribution of several neighboring spots. The inevitable obvious effect of beam scanning is the inhomogeneous dose rate distribution inside the target.[19,20] This technique has already been used with protons for FLASH experiments.[21–23] However, no research has been done on how scanning affects the FLASH effect by comparing the biological outcomes in normal tissue exposed to scanned versus non-scanned FLASH beams. Considering that the exact mechanisms behind the FLASH effect are still unknown, it is unjustified to assume that scanning has no or little impact on the FLASH effect. In order to fill this gap, the impact of various scanning protocols on the FLASH effect should be investigated. This is a vast goal which will take years to complete but is crucial to provide guidance for the use of scanned beams for clinical implementation of FLASH-RT. The first step in tackling this problem is to devise a beam scanning setup and a beam configuration which can then be used for biological FLASH experiments. Here, we propose to use a slit system to simulate the scanning of the FLASH validated electron beam from the eRT6 Oriatron linac. We looked for scanned beam configurations which act (laterally and in depth) as similarly as possible to a single field irradiation. These final configurations were then dosimetrically characterized so that they can later be used for biological FLASH scanning experiments.

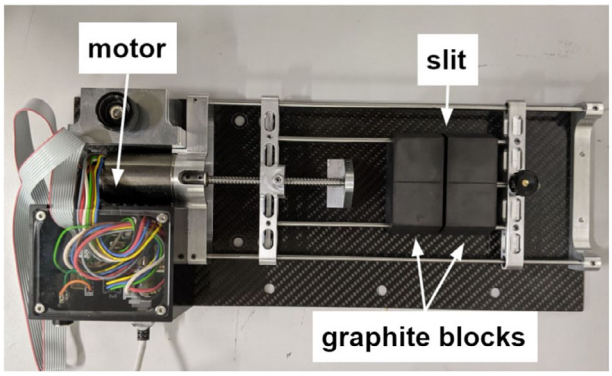

FIGURE 1 Close-up of the slit system. Major parts of the system include two graphite blocks forming a thin slit and the motor that allows movement of the graphite blocks.

2 | MATERIALS AND METHODS

2.1 | Linear accelerator (linac)

The linac used in this project is the Oriatron eRT6 from PMB (PMB, France).[24] The Oriatron eRT6 is a prototype pulsed electron beam linac capable of achieving the high doses per pulse (>10 Gy), and consequently the short irradiation times, required to obtain the FLASH effect, as well as the typical doses per pulse (<0.01 Gy) used in CONV irradiations. The eRT6 is run by a LabVIEW 2014VI (National Instruments, USA) that allows to user to set a pulse width (PW) between 0.5 and 4 μs, a pulse repetition frequency (PRF) between 5 and 250 Hz, the number of pulses, and the electron gun probe voltage between 100 and 300 V. Another parameter the user can change is the effective SSD (source-to-surface distance), which is measured with a telemeter inside the bunker. The notation used for this distance is is the distance displayed on the telemeter in millimeters. The combination of the probe voltage, pulse width, and SSD determines the dose delivered in a single pulse. The energy of the electron beam generated by the Oriatron eRT6 is between 5 and 6 MeV, depending on the electron gun probe voltage.

2.2 | Slit system

The system used to create a slit scanning setup (Figure 1) consists of two 20 mm thick graphite blocks and is connected to a power source and to a computer via USB. The graphite blocks collimate the beam such that only the opening between the two blocks is fully irradiated. This opening—or the slit—can be precisely set using certified gauges to a width of between 0.1 and 6 mm. The two blocks are mounted on a motorized axle that allows the movement of the slit up or down in one direction. The motorization system is composed of

FIGURE 2 Interface of the LabVIEW VI used to control slit motion.

a high-speed DC brushless motor (Maxon Ec-Max30) driving the block assembly via an endless screw. The motor has a maximum speed of 15′000 rpm and provides the necessary speed to move between consecutive linac pulses (mm translation within the ms interval between pulses). By synchronizing the slit motion with the beam pulses, the irradiated field can be spatially segmented. The movement of the slit is controlled by a self-made LabVIEW VI that was created to feature an interface (Figure 2) with three main tabs. On the first tab ("Manual"), the slit can be manually moved with a given speed to either a given absolute position ("Move absolute") or by a given step size ("Move by step") by clicking the corresponding button. With the second tab ("Cyclic"), the slit can be moved between two given absolute positions with a given velocity in a cyclic manner until it is stopped by the user. Clicking the button on this tab once starts the cyclic motion. When the button is clicked a second time, the slit stops at the closest given position. The third tab ("Step by Step") allows the slit to be moved from a given starting position by a given step and velocity, wait for a certain amount of time at that step, take another step, wait again at this step, and so on until the given end position is reached. Besides these three ways of motion, there are additional features on the LabVIEW. There is, for example, the "Enable/Disable" button, which turns the high voltage on or off, and the "Set Pos to 0" button, which zeros the current position. To properly zero the slit, a metallic spacer is used. The spacer is placed at the bottom end of the slit range. The slit is then moved manually when the motor is off until the spacer is reached and then the "Set to 0" button is pressed in the LabVIEW.

2.3 | Dosimetric characterization of the slit system

Dosimetric characterization of the radiation fields produced by the slit system was performed with the use of EBT3 GafChromic films and a virtual water phantom (RW3 slabs, PTW Freiburg). During irradiations, films were placed in the center of the beam at different depths. Each irradiation was repeated three times. Scanning of the irradiated films was done with an Epson V800 flatbed scanner (Epson, USA). The calibration of the films is described in ref. 25. The scanned films were read with the software package Mephysto (PTW, Germany). The absolute doses were read directly for each individual film by averaging the dose per pixel over a user determined region of interest (ROI). Final dose values for PDD profiles were determined as an average of doses measured by three films irradiated in same conditions. Dose uncertainty was calculated as standard deviation of the three dose values. The lateral profiles were smoothed by taking the average of five adjacent profiles, separated by 0.1 mm. The uncertainty of the lateral distance was calculated based on the resolution of the film scans (300 dpi). A low pass filter was applied to the lateral profiles to determine the central flattened region. The flatness F was calculated for unfiltered profiles with the maximum and minimum dose found in the central flattened region, using Equation (1):

$$F = 100 \cdot \frac{D_{max} - D_{min}}{D_{max} + D_{min}} \quad (1)$$

where D_{max} and D_{min} are the maximum and minimum dose values in the central flattened region. The definition of the central flattened region used here is the homogeneous area between 90% isodoses of the smoothed profile obtained with low pass filter.

2.4 | Setup

The setup that was used for testing the slit performance is shown in Figure 3. There is an applicator placed at the exit of the beam to reduce the beam divergence and increase the dose. On the movable irradiation platform there is first the slit system placed vertically, followed directly by a circular graphite collimator (1.7 cm diameter, 2 cm thickness) which is pressed onto the virtual

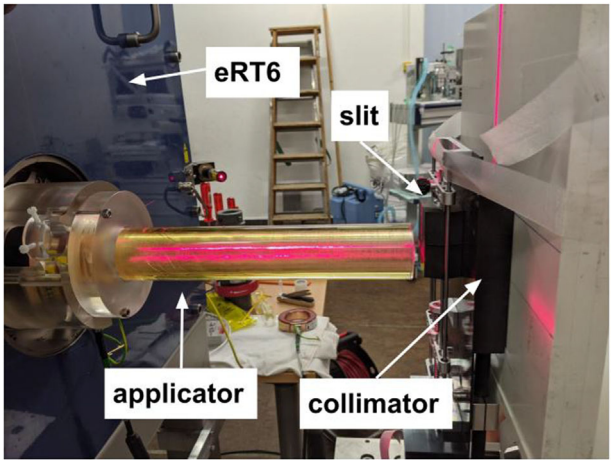

FIGURE 3 Setup used—an applicator is placed at the exit of the linac, followed by the slit system, a 1.7 cm circular carbon collimator, and then the virtual water phantom carrying the EBT3 films.

water surface. Two slit widths were investigated, 1 and 2 mm. The configuration with the 1 mm slit was done at TM350, corresponding to roughly 1.5 Gy/pulse at the surface of the virtual water phantom. The configuration with the 2 mm slit was done both at TM350 and TM490, corresponding, respectively, to roughly 2.3 and 1.5 Gy/pulse at the surface of the water phantom. These combinations of slit widths and SSDs were chosen as a compromise between reducing the slit width in order to increase the number of segmented fields required for covering small pre-clinical targets (5–10 mm) and providing the dose per pulse at the target larger than 1 Gy, which was shown to be the lower limit for the maximal normal brain sparing with pulsed UHDR electron beams.[8] The circular carbon collimator was included to resemble the standard setup used for irradiations of mouse brain and allow for direct comparison of biological results obtained with and without the slit scanning.

2.5 | Optimization of scanning parameters

Optimization was done on the scanning parameters to get a field that resembles a single field non-scanned beam as closely as possible. First, preliminary measurements with a static slit were done to see the effects of the slit on a typical UHDR field. For both slit widths (1 and 2 mm), percentage depth dose (PDD) curves were measured at the previously specified SSDs. The PDD curves were obtained by placing films at depths of 0, 1, 2, 3, 4, 5, 6, 8, and 10 mm in virtual water. Three depths were irradiated at a time – 0, 2, 4 mm; 1, 3, 5 mm; 6, 8, 10 mm. Vertical beam profiles (perpendicular to the slit) at each depth were also obtained. For comparative reasons, a PDD curve and profiles were measured in this same setup at TM490 but without the slit, hereafter known as the open field (OF) setup. The OF setup corresponds to a single field beam.

Surface profiles were obtained by scanning the slit automatically. In order to time the linac pulses properly with the slit motion, this was only done with the cyclic mode. In this case, the ideal step size was translated into a velocity for the slit such that between two pulses the slit moved by one step. The PRF of the beam was set to 50 Hz (20 ms inter-pulse time), as higher frequencies demanded a too high velocity from the slit motor. The slit was set to move cyclically between the two bounds defining the desired irradiated area (such that the entire collimation surface was covered) and a certain number of pulses was irradiated once. The step sizes/slit velocities were optimized in each configuration to give the flattest scanned beam profiles by measuring the flatness of the surface profiles for different slit velocities. It was expected that the optimal step sizes were of the order of the slit widths and these values were taken as a starting point. Only surface profiles were considered for optimization of the scanning velocity since we assumed (and later confirmed) that the beam flatness improves with depth due to scattering, being therefore the worst at the surface.

2.6 | Final beam characterization

Once the optimal velocity was found for each configuration, a complete beam characterization was done by measuring a PDD (following the same procedure as before for static slit cases) and taking the profiles at 0, 2, and 4 mm depth in virtual water.

3 | RESULTS

3.1 | Scanning parameter optimization

The measured doses per pulse at the surface are 1.58 ± 0.03 Gy/pulse for the 1 mm static slit at TM350, 2.32 ± 0.05 Gy/pulse for the 2 mm static slit at TM350, and 1.50 ± 0.03 Gy/pulse for the 2 mm static slit at TM490. The TM350 is the closest distance from the machine where we could put the slit system with the carbon collimator since at this distance the collimator was almost in contact with the applicator. Therefore, the doses per pulse obtained for TM350 are the highest that can be achieved for the given slit widths. The PDDs of the static slit in the three configurations and the OF PDD are shown in Figure 4. The lateral profiles in depth of the 1 mm and the 2 mm static slits at TM490 are shown in Figure 5.

An example of the tuning of the slit velocity that was done to find the most homogeneous surface profile is shown in Table 1 for the 2 mm slit at TM350. An initial

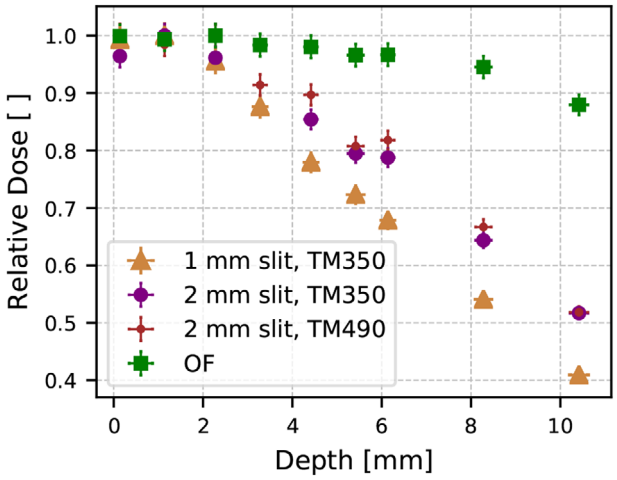

FIGURE 4 PDDs of the two static slits (1 mm and 2 mm) at the distances (SSDs) used for obtaining the final scanning configurations compared to the PDD of the OF.

TABLE 1 Flatness values (F) for profiles found with various slit scanning velocities for the 2 mm slit at TM350.

Slit velocity [mm/s]	F
90	7.68%
100	8.47%
110	6.54%

The profile obtained with scanning velocity of 110 mm/s has the smallest F value indicating the smoothest profile. This was also confirmed by visual inspection of the irradiated films.

guess of the optimal slit velocity was made by calculating the velocity that corresponds to the movement of the slit by the distance equal to its width during the time between two consecutive pulses (20 ms). For 2 mm slit this gives a velocity of 100 mm/s. Beam profiles were then generated at slit velocities ranging from 80 to 120 mm/s (velocity was changed in steps of 10 mm/s within this range) and the optimal velocity was chosen as the one giving the flattest dose profile. Irradiated films were inspected visually for overlaps or gaps between adjacent steps (visible as darker or lighter periodically repeating lines), which are an indicator of too low or too high slit velocity. Beam flatness defined by Equation (1) was used as a merit for numerical comparison of the obtained profiles. The total number of pulses was chosen such that the overall dose was around 10 Gy and the same number of pulses was delivered for each step. The 90 mm/s profile and the 100 mm/s profile are both examples of profiles of automatic scanning with a too low velocity, resulting in overlaps between adjacent steps. These overlaps were more visible on the film directly but can also be seen by a flatness value which is higher for the two lower slit velocities. Dosimetric parameters and optimal scanning slit velocities found for each configuration are summarized in Table 2. Two dose rate values were calculated as well based on the dose per pulse and absorbed dose in one scan, both at the surface level. Considering the ambiguity in calculation of the dose rate for scanned beams, which will be addressed in the Discussion, these two values represent the highest and the lowest dose rate metrics attributable to the final scanning configurations.

3.2 | Final beam characterization

The PDDs found for the 1 mm slit at TM350 scanned at 50 mm/s and the static 1 mm slit at TM350 are compared to the OF beam PDD in Figure 6. Integrating the PDDs up to 4 mm using the composite trapezoidal rule gives 90.0%, 92.2%, and 96.0% of the maximum dose for the static slit, the scanned slit, and the OF configurations, respectively. Integrating the PDDs up to 10 mm gives 72.45%, 87.64%, and 95.13% of the maximum dose for the static slit, the scanned slit, and the OF configurations, respectively. The lateral profiles at 0, 2, and 4 mm depths for the scanned 1 mm slit at TM350 are shown in Figure S1. The PDDs found for the 2 mm slit at TM490 scanned at 110 mm/s and the static 2 mm slit at TM490 are compared to the OF beam PDD in Figure 7. Integrating the PDDs up to 4 mm using the composite trapezoidal rule gives 93.1%, 94%, and 96.0% of the maximum dose for the static slit, the scanned slit, and the OF configurations, respectively. Integrating the PDDs up to 10 mm gives 80.69%, 90.25%, and 95.13% of the maximum dose for the static slit, the scanned slit, and the OF configurations, respectively. The lateral profiles at 0, 2, and 4 mm depths for the scanned 2 mm slit (TM490) are shown in Figure S2. The PDDs found in for the 2 mm slit at TM350 scanned at 110 mm/s and the static 2 mm slit at TM350 are compared to the OF beam PDD in Figure 8. Integrating the PDDs up to 4 mm using the composite trapezoidal rule gives 91.5%, 94.8%, and 96.0% of the maximum dose for the static slit, the scanned slit, and the OF configurations, respectively. Integrating the PDDs up to 10 mm gives 78.8%, 92.2%, and 95.1% of the maximum dose for the static slit, the scanned slit, and the OF configurations, respectively. The lateral profiles at 0, 2, and 4 mm depths for the scanned 2 mm slit (TM350) are shown in Figure S3.

The values found by integrating the PDDs up to 4 and 10 mm for final scanning configurations and OF are summarized in Table 3. For comparative purposes, the profiles at 0, 2, and 4 mm depths for the OF beam are shown in Figure S4. An overlap of the profiles of the three final configurations and the OF beam at 0, 2, and 4 mm depths is shown in Figure 9.

4 | DISCUSSION

The main goal of the study is to evaluate the feasibility of using a simple slit scanning device to generate

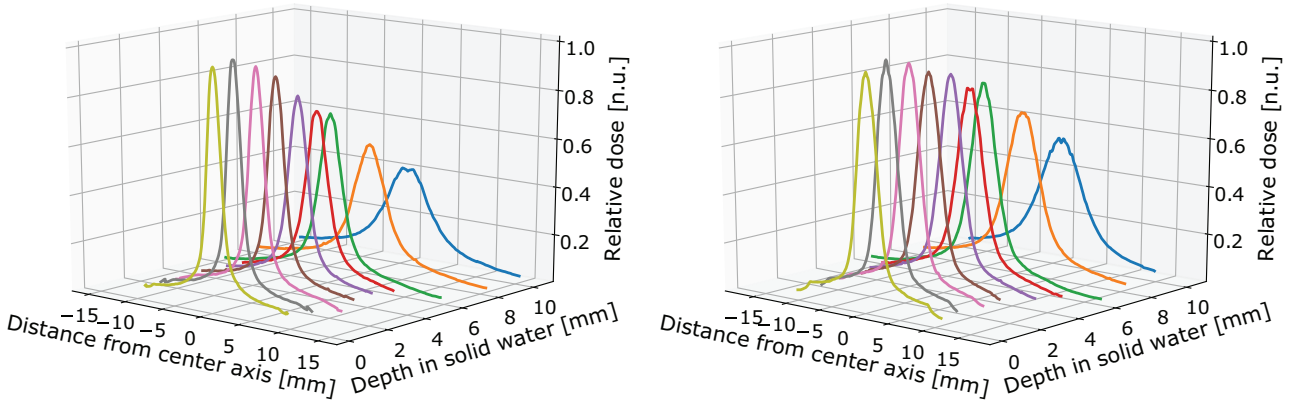

FIGURE 5 Left: The profiles in depth (0–10 mm) for the 1 mm static slit at TM350. Right: The profiles in depth (0–10 mm) for the 2 mm static slit at TM490.

TABLE 2 Overview of the parameters found for each of the final scanning configurations.

Slit width	Dose per pulse [Gy/pulse]	Pulse dose rate [10^5 Gy/s]	Slit velocity [mm/s]	Dose in one scan [Gy]	Av. dose rate in one scan [Gy/s]
1 mm (TM350)	1.58 ± 0.03	9.0 ± 0.1	50	3.0 ± 0.1	15
2 mm (TM350)	2.32 ± 0.05	13.0 ± 0.2	110	3.7 ± 0.2	41
2 mm (TM490)	1.50 ± 0.03	8.5 ± 0.1	110	2.4 ± 0.1	27

Dose and dose rate values are reported for the surface. Dose per pulse represents the dose delivered by a single pulse passing through the slit. Pulse width was set to 1.8 μs. Dose in one scan represents the average dose delivered by one passage of the slit over the target. This dose is the sum of the dose contributions from several neighboring slit positions (each delivering one pulse) and is therefore larger than the dose per pulse. Average dose rate in one scan represents the ratio between the dose delivered in one scan and the time required to finish one scan.

TABLE 3 Summary of the integral PDD values found for the three final scanning slit configurations and the OF configuration shown as a percentage of the maximum dose.

	1 mm slit at TM350	2 mm slit at TM490	2 mm slit at TM350	Open field
Integral of the PDD up to 4 mm depth as percentage of maximal dose	92.2%	94.0%	94.8%	96.0%
Integral of the PDD up to 10 mm depth as percentage of maximal dose	87.6%	90.3%	92.2%	95.1%

Integrations of the PDDs were performed up to 4 and 10 mm depths.

a scanned electron FLASH beam. From the results of using a single static slit, it is obvious that placing a slit in the middle of an electron beam has several non-negligible effects on the beam. One effect is the strong reduction of the dose per pulse: the smaller the slit, the stronger the dose per pulse reduction. For 1 mm at the closest SSD the dose per pulse is just above 1 Gy. Without the slit, at the same SDD the dose per pulse is above 5 Gy. Radiobiological studies indicated dose per pulse and dose rate as critical FLASH beam parameters. We decided not to use slit sizes smaller than 1 mm to keep the dose per pulse above 1 Gy, which was validated to reproduce the FLASH effect.[8] Scanned beam delivery can be characterized by different dose rate metrics, most of which require the use of simulation algorithms to account for the overlaps of dose contributions from several radiation fields. Such calculations go beyond the scope of this study and will be highly dependent on the applied scanning protocol. For example, the total dose can be delivered with our scanning slit system in a single sweep mode, which assumes waiting at each step until the total number of pulses required for a given dose is reached and then moving the slit to the next step. Another approach would be to deliver the dose by repetitive scanning overt the target, which assumes that the slit is scanned across the beam continuously back and forth, delivering a single pulse at each step. The latter will have significantly lower per spot dose rate values. In Table 2 we have reported only the two simple to calculate dose rate metrics for each of the final scanning configurations. The pulse dose rate, obtained by dividing the dose per pulse by the pulse width is the highest dose rate value that can be associated with each scanning configuration. On the contrary, the average dose rate in

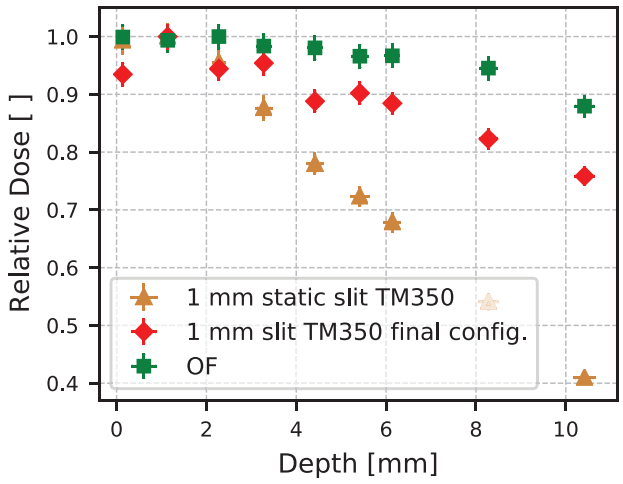

FIGURE 6 Comparison of PDDs obtained with the static 1 mm slit at TM350, the scanned 1 mm slit at TM350 and the OF beam.

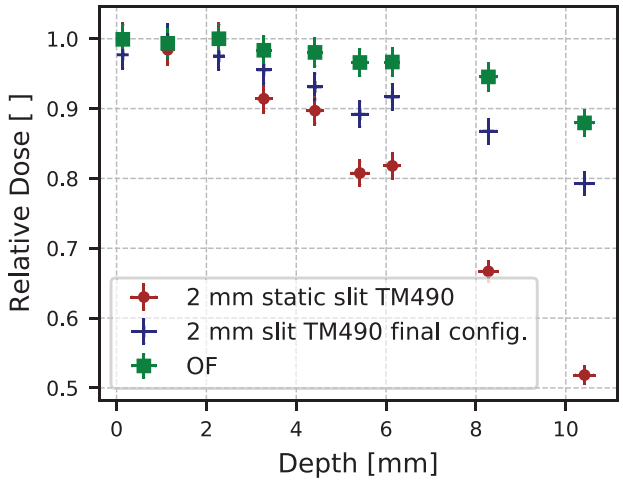

FIGURE 7 Comparison of PDDs obtained with the static 2 mm slit at TM490, the scanned 2 mm slit at TM490, and the OF beam.

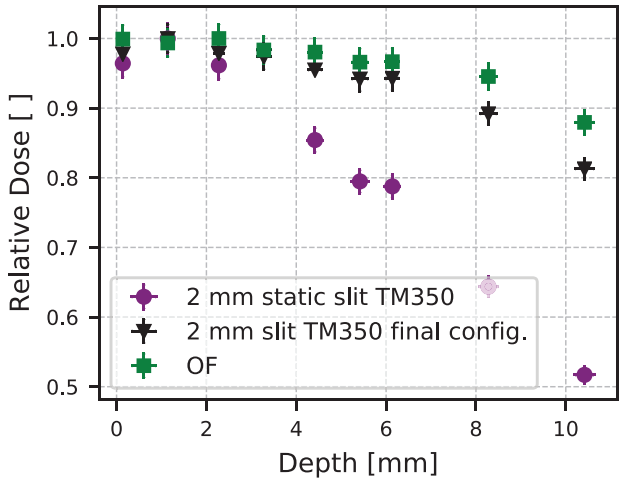

FIGURE 8 Comparison of PDDs obtained with the static 2 mm slit at TM350, the scanned 2 mm slit at TM350 and the OF beam.

a single sweep, obtained by dividing the total dose delivered in one scan by the time required for one scan, is the lowest dose rate metric attributable to the scanned beam.

Another effect of placing the narrow slit in front of the electron beam is the change of the PDD of the beam. As can be seen in Figure 4, the PDD of a beam passing through a single static slit is completely different than the PDD of an OF beam. The OF PDD has a plateau, where for several millimeters the dose stays approximately the same whereas the static slit PDDs almost immediately decrease in dose. This plateau is key in experiments as similar doses are desired for thicknesses that vary by a few millimeters. Typically, electron beams suffer from a strong field size effect, due to loss of electron equilibrium. We believe that the limited field size in one direction is causing the observed sharp PDD drop. The electron equilibrium cannot be established and the dominant effect remains widening of the beam, which leads to a faster decrease of the dose with depth.

We attempted to find a scanning slit setup that closely resembles an OF beam, which is a prerequisite for studying the effects of scanned versus non-scanned FLASH beam. In the final scanned beam characterization, the PDDs of beams obtained by scanning the slit come close to reconstructing the PDD of the OF beam (Figures 6–8). The reconstructions of the PDDs with the scanned slits are quantified by the integrals up to 4 and 10 mm that were calculated. These two depths represent, respectively, the thickness of thinner targets, for example, skin and subcutaneous tumors, and thicker targets, for example, mouse brain and lungs. The difference between the OF PDD integrals and the integrals found in the final configurations up to 4 and 10 mm depth for automatic scanning differ only by around 2%–4% and up to 7.5%, respectively. The benefit of having an almost reconstructed PDD is that the plateau useful for experiments is once again obtained. We hypothesize that the cause for the remaining difference between the OF and scanning beam PDDs are low energy electrons scattered from the slit. Because of the short range is in medium, scattered electrons deposit dose at lower depths only, reducing PDD values at higher depths.

The flatness of the lateral beam profiles at the surface obtained with the final scanning configurations (Figures S1–S3) is comparable to that of the OF beam (Figure S4), as seen by the values of flatness (F) that were calculated and specified on the figures. The flatness of the profiles gets further improved with depth. Finally, as observed from Figure 9, the profiles measured for all three final scanning configurations match the shape of the OF profile in the 1 cm region around the beam central axis. The difference appears at the edges where the scanning beam profiles show about 10 % reduction compared to the OF beam. This was expected due to worse alignment of the off-center beam and the slit, resulting in more electrons being stopped by the

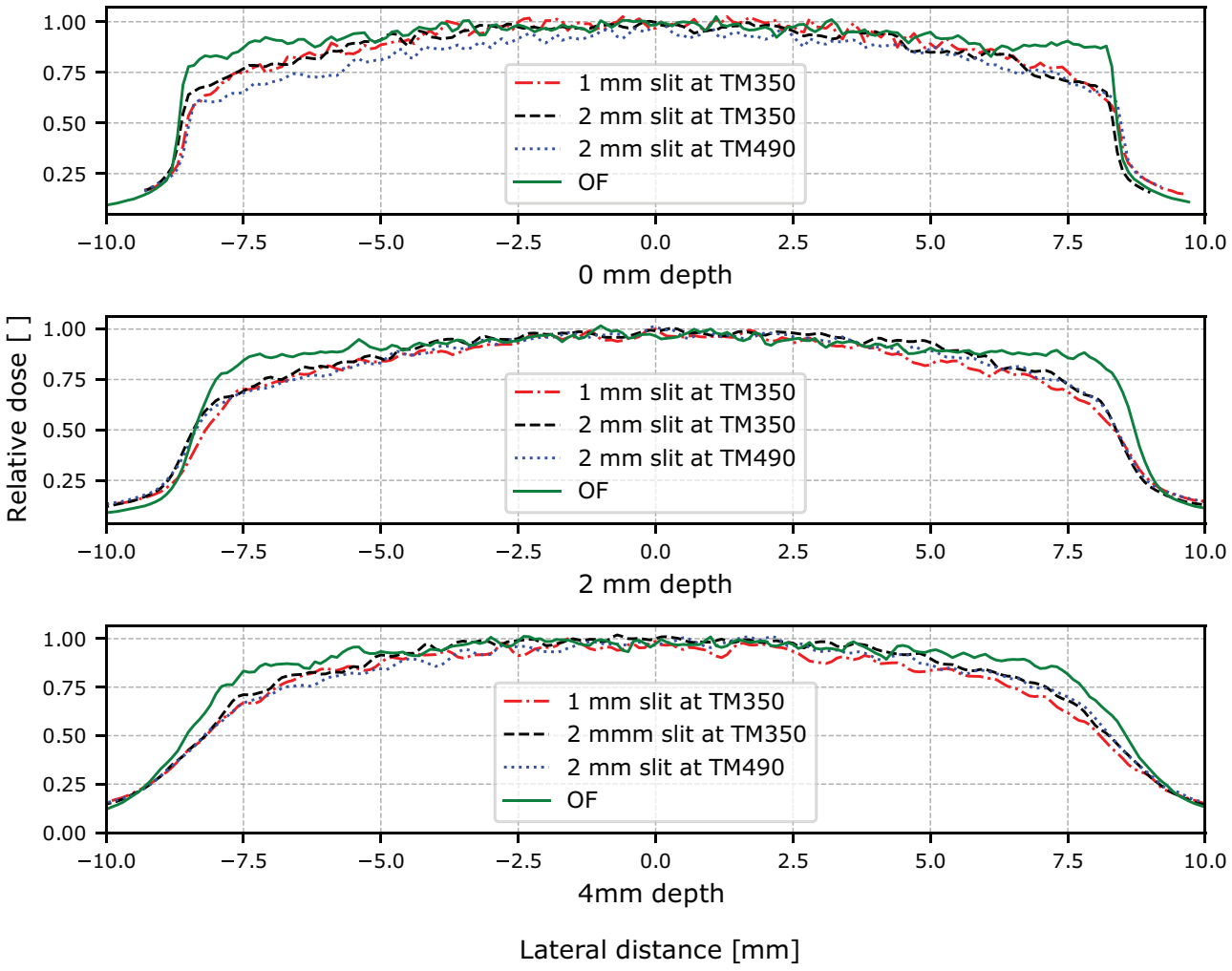

FIGURE 9 Comparisons of the lateral beam profiles for the three final scanning configurations and the OF beam and 0–4 mm depths.

carbon blocks the further the slit is displaced from the beam axis. However, field sizes of 1 cm are sufficient for irradiating most of the targets in small animals.

5 | CONCLUSIONS

We have constructed a motorized slit system that is able to spatially modulate the FLASH validated beam (Oriatron eRT6) by scanning a narrow slit across the beam. It can do so at high translational velocities, which allows to change the position of the slit between two consecutive linac pulses arriving at the frequency of 50 Hz. The capability of the slit system to recreate an open field irradiation while maintaining high dose per pulse required in FLASH-RT was confirmed with three different automatic scanning configurations (1 mm slit at TM350, 2 mm slit at TM350, and 2 mm slit at TM490). The obtained radiation fields were characterized with PDDs and lateral profiles at various depths. The three scanning slit configurations were found to give homogeneous surface lateral profiles with calculated beam flatness comparable to the non-scanned open field configuration. As expected, the homogeneity of lateral profiles increased with depth in medium. While the presence of the static slit drastically deteriorated the open field PDD, scanning of the slit at optimal velocity almost fully reconstructed the open field PDD. Using these fully characterized setups, it is now possible to implement different scanning protocols with our FLASH validated beam and investigate the impact of scanned beam delivery on the magnitude of the FLASH effect. Such studies are crucial for understanding the temporal requirements that have to be met when beam scanning is used to administer FLASH-RT on large targets.

ACKNOWLEDGMENTS

Parts of this study were included in the master thesis "Dosimetric characterization of radiation fields produced by a motorized slit system" by Roxane Oesterle, defended in 2022 at École Polytechnique Fédérale de Lausanne, Lausanne, Switzerland. The study was partly

supported by a Sinergia grant (FNS CRS II5_186369), an NIH program project grant PO1CA244091, and from the funding of project 18HLT04 UHDpulse from the EMPIR program co-financed by the Participating States and from the European Union's Horizon 2020 research and innovation program.

Open access funding provided by Universite de Lausanne.

CONFLICT OF INTEREST STATEMENT

None.

REFERENCES

1. Vozenin MC, Montay-Gruel P, Limoli C, Germond JF. All irradiations that are ultra-high dose rate may not be FLASH: the critical importance of beam parameter characterization and in vivo validation of the FLASH effect: An introduction letter. *Radiat Res*. 2020;194:571-572.
2. Favaudon V, Caplier L, Monceau V, et al. Ultrahigh dose-rate FLASH irradiation increases the differential response between normal and tumor tissue mice. *Sci Transl Med*. 2014;6:245ra93.
3. Vozenin MC, Hendry JH, Limoli CL. Biological benefits of ultra-high dose rate FLASH radiotherapy: sleeping beauty awoken. *Clin Oncol (R Coll Radiol)*. 2019;31:407-415.
4. Fouillade C, Curras-Alonso S, Giuranno L, et al. FLASH irradiation spares lung progenitor cells and limits the incidence of radio-induced senescence. *Clin Cancer Res*. 2020;26:1497-1506.
5. Pratx G, Kapp DA. Ultra-high-dose-rate FLASH irradiation may spare hypoxic stem cell niches in normal tissues. *Int J Radiat Oncol Bio Phys*. 2019;105:190-192.
6. Esplen N, Mendonca MS, Bazalova-Carter M. Physics and biology of ultrahigh dose-rate (FLASH) radiotherapy: a topical review. *Phys Med Biol*. 2020;65:23TR03.
7. Montay-Gruel P, Acharya MM, Petersson K, et al. Long-term neurocognitive benefits of FLASH radiotherapy driven by reduced reactive oxygen species. *Proc Natl Acad Sci USA*. 2019;116:10943-10951.
8. Montay-Gruel P, Petersson K, Jaccard M, et al. Irradiation in a flash: unique sparing of memory in mice after whole brain irradiation with dose rates above 100 Gy/s. *Radiother Oncol*. 2017;124:365-369.
9. Montay-Gruel P, Bouchet A, Jaccard M, et al. X-rays can trigger the FLASH effect: ultra-high dose-rate synchrotron light source prevents normal brain injury after whole brain irradiation in mice. *Radiother Oncol*. 2018;129:582-588.
10. Alaghband Y, Cheeks SN, Allen BD, et al. Neuroprotection of radiosensitive juvenile mice by ultra-high dose rate FLASH irradiation. *Cancers (Basel)*. 2020;12:1671.
11. Levy K, Natarajan S, Wang J, et al. Abdominal FLASH irradiation reduces radiation-induced gastrointestinal toxicity for the treatment of ovarian cancer in mice. *Sci Rep*. 2020;10:21600.
12. Loo BW, Schuler E, Lartey F, et al. Delivery of ultra-rapid FLASH radiation therapy and demonstration of normal tissue sparing after abdominal irradiation of mice. *Int J Radiat Oncol Biol Phys*. 2017;98:E16-E16.
13. Hornsey S, Bewley DK. Hypoxia in mouse intestine induced by electron irradiation at high dose-rates. *Int J Radiat Biol Relat Stud Phys Chem Med*. 1971;19:479-483.
14. Soto LA, Casey KM, Wang J, et al. FLASH irradiation results in reduced severe skin toxicity compared to conventional-dose-rate irradiation. *Radiat Res*. 2020;194:618-624.
15. Pawelke J, Brand M, Hans S, et al. Electron dose rate and oxygen depletion protect zebrafish embryos from radiation damage. *Radiother Oncol*. 2021;158:7-12.
16. Vozenin MC, De Fornel P, Petersson K, et al. The advantage of FLASH radiotherapy confirmed in mini-pig and cat-cancer patients. *Clin Cancer Res*. 2019;25:35-42.
17. Bourhis J, Sozzi WJ, Jorge PG, et al. Treatment of a first patient with FLASH-radiotherapy. *Radiother Oncol*. 2019;139:18-22.
18. Kooy HM, Clasie BM, Lu HM, et al. A case study in proton pencil-beam scanning delivery. *Int J Radiat Oncol Biol Phys*. 2010;76:624-630.
19. van Marlen P, Dahele M, Folkerts MEA. Bringing FLASH to the clinic: treatment planning considerations for ultrahigh dose-rate proton beams. *Int J Radiat Oncol Biol Phys*. 2020;106(3):621-629.
20. van de Water S, Safai S, Schippers JM, et al. Towards FLASH proton therapy: the impact of treatment planning and machine characteristics on achievable dose rates. *Acta Oncologica*. 2019;58(10):1463-1469.
21. Cunningham S, McCauley S, Vairamani K, et al. FLASH proton pencil beam scanning irradiation minimizes radiation-induced leg contracture and skin toxicity in mice. *Cancers*. 2021;13:1012.
22. Rama N, Saha T, Shukla S, et al. Improved tumor control through t-cell infiltration modulated by ultra-high dose rate proton FLASH using a clinical pencil beam scanning proton system. *Int J Radiat Oncol Biol Phys*. 2019;105:S164-S165.
23. Diffenderfer ES, Verginadis II, Kim MM, et al. Design, implementation, and in vivo validation of a novel proton FLASH radiation therapy system. *Int J Radiat Oncol Biol Phys*. 2020;106:440-448.
24. Jaccard M, Durán MT, Petersson K, et al. High dose-per-pulse electron beam dosimetry: commissioning of the Oriatron eRT6 prototype linear accelerator for preclinical use. *Med Phys*. 2018;45:863-874.
25. Jaccard M, Petersson K, Buchillier T. High dose-per-pulse electron beam dosimetry: usability and dose-rate independence of EBT3 Gafchromic films. *Med Phys*. 2017;44(2):725-735.

SUPPORTING INFORMATION

Additional supporting information can be found online in the Supporting Information section at the end of this article.

How to cite this article: Oesterle R, Bailat C, Buhlmann D, Bochud F, Grilj V. Construction and dosimetric characterization of a motorized scanning-slit system for electron FLASH experiments. *Med Phys*. 2024;51:1396–1404. https://doi.org/10.1002/mp.16610